Stress Corrosion Susceptibility of Stress-Coined Fastener Holes in Aircraft Structures

Aubrey E. Carter* and Sathya Hanagud†
Georgia Institute of Technology, Atlanta, Ga.

The cold working process of stress coining is used to provide fatigue improvement of fastener holes in aircraft structures. The cold working produces a radial flow of the metal. The residual stresses resulting from stress coining provide protection against fatigue damage by opposing the applied tensile stresses in service at the edge of the fastener hole. However, it is shown in this paper that in addition to the compressive stresses surrounding the stress coined hole, there are tensile stresses that result from the coining operation and that these residual tensile stresses can have a deleterious effect on the stress corrosion susceptibility of the postcoined structure.

Introduction

AIRCRAFT structural members are susceptible to fatigue cracking at fastener holes under cyclic loading conditions.[1] Many aircraft parts containing fastener holes are stress coined prior to assembly, or subsequently, to lower this susceptibility to cracking in fatigue-prone areas.[2] Stress coining is a cold working process that consists of expanding holes in structural members by pulling an oversized mandrel hydraulically through the fastener holes, as illustrated in Fig. 1.

The process of drawing the mandrel through the fastener holes results in a radial flow of the metal. The residual stresses resulting from the operation in the region surrounding the holes provide protection against fatigue damage by opposing the applied tensile stresses.[3] As shown in this paper, there is a zone under sustained tensile stress adjacent to the compressively stressed region. Although the tensile stress does not affect the fatigue properties of the part, its deleterious effect on the stress corrosion susceptibility of high-strength aluminum alloys under adverse grain orientation can result in cracking of parts in service.

In particular, the problem of the susceptibility to stress corrosion cracking of AISI 7075-T651 aluminum alloy, a commonly used aircraft high-strength structural material, has been examined theoretically and experimentally. The elastic-plastic analysis shows that the short transverse stress corrosion threshold level is exceeded by the residual stresses produced by the stress coining process. Alternate immersion corrosion testing, metallographic examination, and electron fractography have been used to investigate the stress corrosion susceptibility experimentally.

Experimental Procedures

Material

Many load-carrying members of structural assemblies in aircraft are machined from high-strength aluminum alloy plate shock. For optimim static tensile properties, the longitudinal direction of the plate is usually aligned with the principal tensile stress direction of the structure.[4] Structures with the rolling direction aligned in this manner benefit from grain size strengthening caused by the smaller effective grain size.[5] Structures stressed perpendicular to the rolling direction are weakened by the alignment of inclusions in the longitudinal direction and by the larger grain size.

Therefore, for common structural cross section shapes (such as I-beams with their axes aligned with the rolling direction), the fastener holes may be located in the longitudinal short transverse plane, as illustrated in Fig. 2. When these fastener holes are stress coined, the sustained tensile stresses do not result from the coining process in short transverse grains. As shown in this paper, these stresses may exceed the threshold stress to cause stress corrosion cracking in short transverse smooth specimens of AISI 7075-T651 aluminum which is a commonly used aircraft high-strength structural material.[6] The susceptibility to stress corrosion cracking of such a structural element has been studied and reported in this paper by using alternate immersion corrosion testing per ASTM G 31-72.[7]

Test Specimens

Test specimens were machined from plate stock. As shown in Fig. 3, grain orientation was longitudinal-short transverse. Specimen microstructure is shown in Fig. 4. From between five to eight 0.249/0.250-in. holes were drilled in each specimen with hole spacing varying between 1/2-1-1/4 in. The inside surfaces of the holes were honed to obtain a 32 rms surface finish. Eight such specimens were prepared.

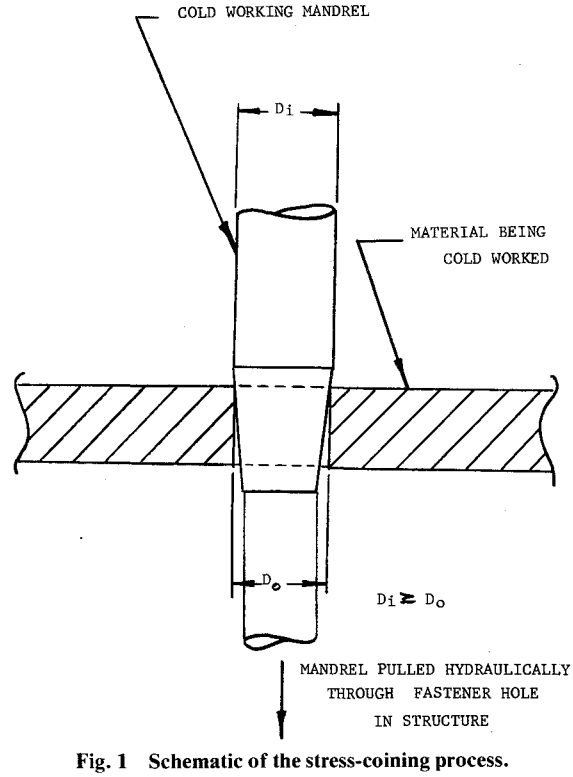

Fig. 1 Schematic of the stress-coining process.

Received January 9, 1974; revision received June 26, 1974. This work was supported by NASA Grant NGR-11-002-169.

*Graduate Student, School of Aerospace Engineering.
†Professor, School of Aerospace Engineering.

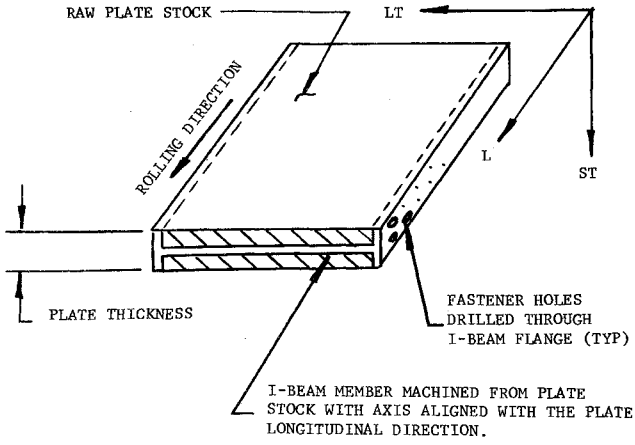

A) ORIENTATION OF MACHINING TYPICAL AIRCRAFT "I-BEAM" STRUCTURE.

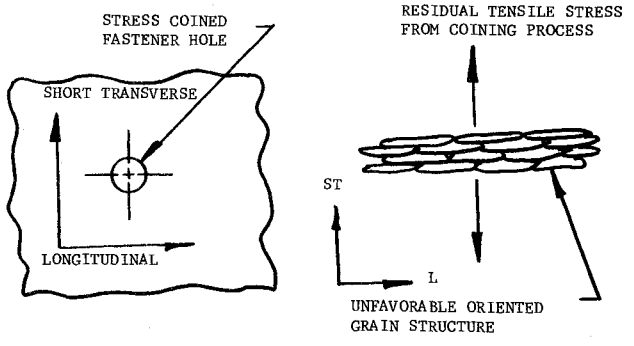

B) DETAIL OF TYPICAL FASTENER HOLE.

C) DIRECTION OF GRAIN STRESSING AROUND COINED FASTENER HOLE.

Fig. 2 Typical aircraft structural part machined from plate stock.

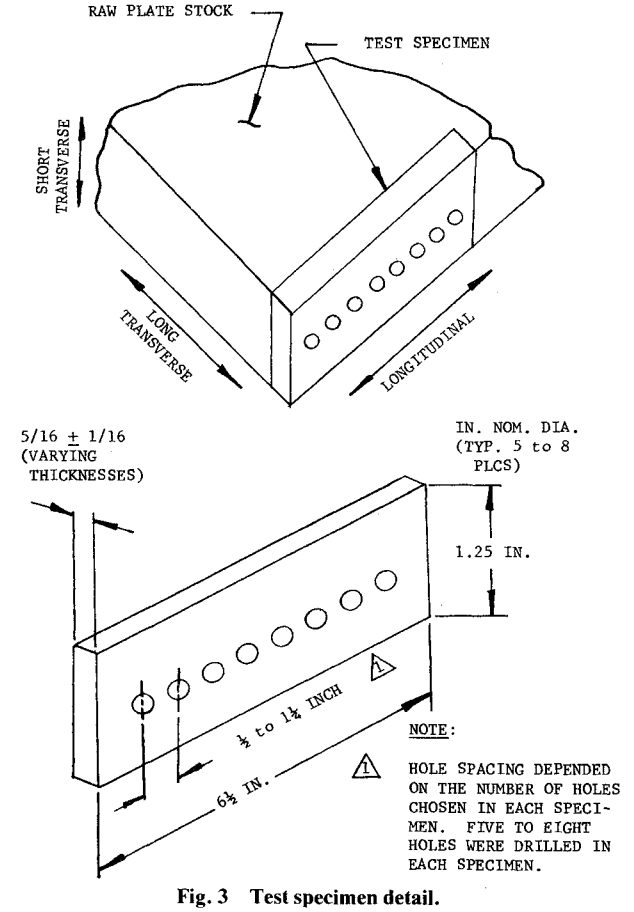

Fig. 3 Test specimen detail.

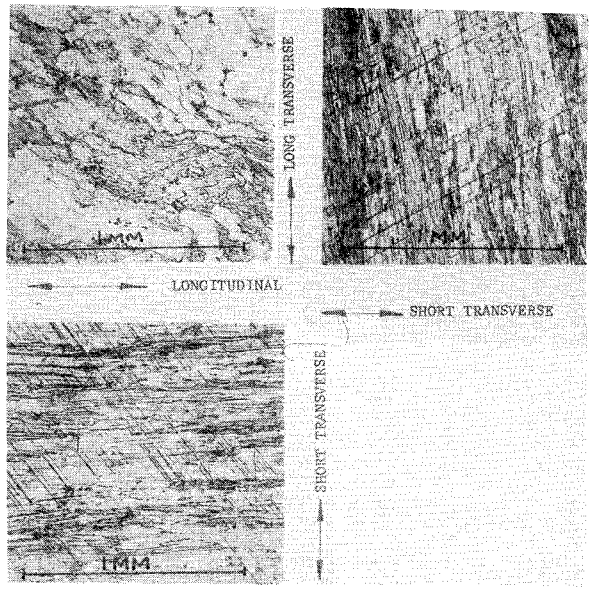

Fig. 4 Test specimen grain structure.

Stressing of the Specimen

No external load was applied to the test specimens during the test duration. Prior to testing, the holes in five specimens were stress coined by expanding the holes by drawing an oversize cold working mandrel through the holes.‡ The holes were expanded by 0.006 in. on the diameter (with mandrel inserted), which resulted in an after coining hole size of 0.253/0.254 in. (with mandrel withdrawn). The resultant residual stress analysis has been discussed in the appendix. One specimen was used as a control, with only holes drilled (no cold working). All specimens were vapor degreased and wiped with acetone-soaked cotton after stressing, and immediately placed in the test chamber.

Test Equipment

Alternate immersion of the specimens was accomplished by movement of the salt solution. At the beginning of the immersion cycle, the solution was contained in a lower tank. The cycles were controlled by a timer-actuated solenoid valve which caused air to enter the reservoir tank. The rising pressure caused the salt solution to flow into the test chamber, where the test specimens were suspended. The second timer signal closed the solenoid valve, stopping the flow of air into the tank. The tank pressure then slowly decreased to atmospheric pressure by continual leakage from a bleeder valve, and the salt solution flowed back into the reservoir tank. The cycle was timed for 10 min immersion of the test specimens in the salt solution, followed by 50 min air-drying time.

Test Medium

The test solution was 3.5% sodium chloride (by weight) and distilled water prepared weekly. The salinity of the solution was checked each day using a hydrometer, and distilled water was added as necessary to compensate for evaporation. Solution pH was maintained at 6.4-7.2. Air temperature in the test chamber was maintained at 78-82°F, with a relative humidity of 45%. This test solution complies with the test medium requirements of the Federal Test Method Standard No. 151b, Method 823, "Stress Corrosion for Aluminum alloy Plate, Extrusions, and Forgings by Alternate Immersion."[8]

‡The test specimens were stress coined using cold working mandrels designed by the authors.

Test Duration

The stress-coined specimens were placed in the alternate immersion corrosion test chamber for 42 days. The specimens were visually examined every second day, using a 10X magnifying glass to detect macrocrack initiation. When cracks were detected, the time and location of the crack was recorded, and the specimen was placed back in the test chamber for continuance of the test.

Metallographic Examination

Before subjecting the specimens to alternate immersion tests, a stress coined specimen and an uncoined test specimen were sectioned perpendicular to the specimen holes, mounted, and metallographically polished by using a magnesium oxide slurry. The specimens were then etched with Kellers Reagent consisting of 1% HF, 1.5% Hcl, 2.5% HNO_3, and 95% distilled water. The cross sections were then examined, using an optical microscope, to compare the microstructure surrounding the coined and uncoined holes. Photomicrographs of the precoined hole and postcoined hole are shown in Fig. 5. After the immersion tests, the specimens were subjected to visual analysis, examination by optical microscope and electron fractography studies. Results are discussed in the next section.

Test Results

Specimens Before Immersion Tests

The following observations can be noted as a result of the examination of micrographs before immersion tests. In contrast to the straight and lamellar structure of the uncoined grains, the cold worked grain structure of the stress coined hole exhibited bulging of the grains caused by the local yielding of the hole inside diameter as can be seen in Fig. 5. Severe grain distortion is visible at the hole-mandrel interface.

Visual Analysis After Immersion Tests

All the test specimens exhibited corrosion pitting and oxidation by-products on the surfaces of the test specimens. Macrocracking was visible near the holes in two of the five stress-coined specimens. The cracking was aligned perpendicular to the specimen short transverse grain direction in each case. The crack sizes varied in length from 1/16-1/2 in. A stress coined test specimen with visible cracks is shown in Fig. 6. This figure shows the prescence of macrocracks in the vicinity of three of the cold worked holes. Cracking was first visually detected after 23 days of alternate immersion and 3.5% NaCl exposure. The entire test specimen surface was covered with corrosion products.

The largest crack was broken open for analysis and confirmation of the fracture mode. A well-defined precracked region of slow growth was visible, originating symmetrically between two of the stress coined holes and propagating toward the holes. This region had a "flaky" appearance darkened by corrosion products, in contrast to the clean and moderately rough texture produced by the opening of the crack after the test for fracture analysis. The precrack had penetrated through approximately 80% of the net section, as shown in Fig. 7. Slow growth region can be distinguished from rapid fracture area. Circles identified by letters D, E, F have been examined by electron fractography. No visible cracking existed in the uncoined control specimen.

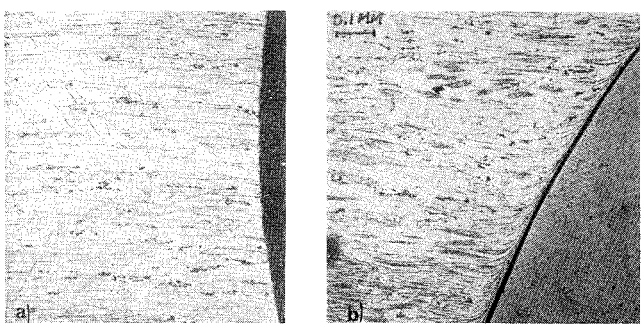

Fig. 5 Comparison of a) precoined and b) post-coined microstructure.

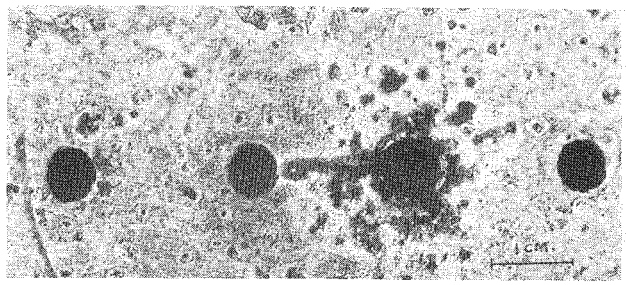

Fig. 6 Test specimen with visible cracks.

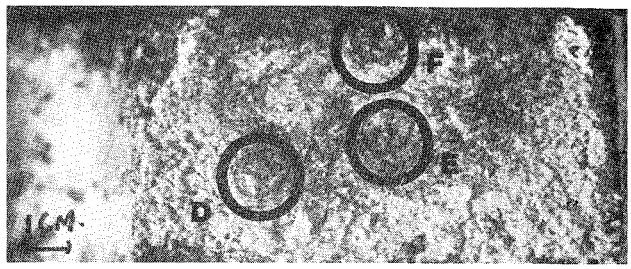

Fig. 7 Photomacrograph of section through the visible crack.

Fig. 8 Details of cross section through the visually observed surface crack etched with Keller's regeant.

Optical Microscopic Examination

The surfaces of the uncoined control specimen and cross sections cut parallel to the short transverse direction were examined microscopically. No microcracking was detected.

The largest crack observed in the stress coined specimen during the alternate immersion test was sectioned through the crack origin for microscopic examination. The crack originated from the root of a corrosion pit and propagated intergranularly.Multiple secondary intergranular cracks from the corrosion pit were also present. The corrosion attack was preferentially oriented along the grain boundaries. Photomicrographs of the etched cross section is shown in Fig. 8.

Electron Fractography

The following discussion refers to the examination of test specimens 2 and 3 by a scanning electron microscope. The crack origin was scanned to determine the mode of cracking at the fracture nucleus. The area was covered with corrosion products, with cracks in the corrosion products, giving the

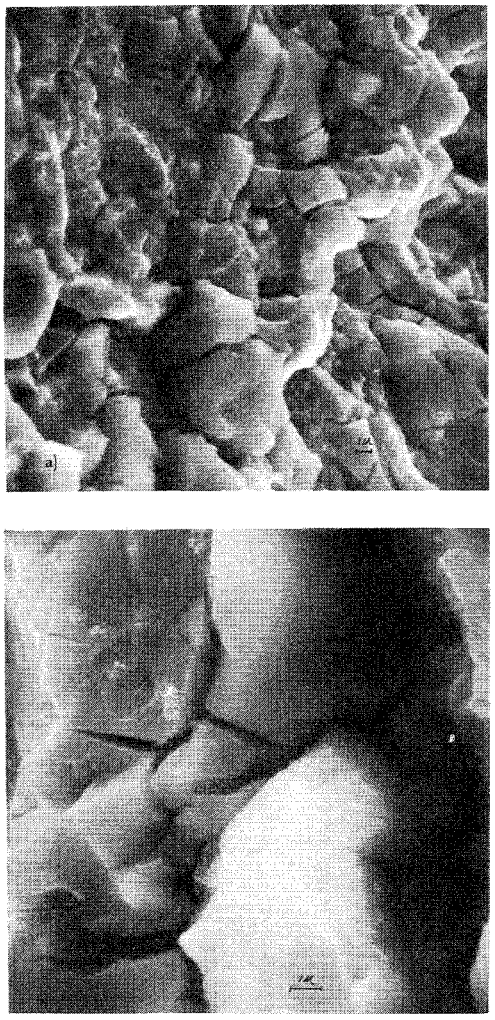

Fig. 9 Electron fractograph.

surface a typical "mud crack" appearance of stress corrosion cracking, as shown in Fig. 9a. The crack path was intergranular with multiple secondary intergranular cracking. Multiple secondary cracking is typical of stress corrosion cracking and is not usually observed in other types of intergranular cracking.[9] The crack transition was characterized by the presence of equiaxed dimples produced by the tensile overstress induced to open the crack for examination, and contrasted vividly with the well-faceted grain structure characteristic of the stress corrosion region, as depicted in Fig. 9b.

Discussion of Results

The stress distribution resulting from the stress coining process is analyzed in the Appendix. Significant results can be summarized as follows. The residual stresses σ_r and σ_θ in the material after the stress coining operation are

$$\sigma_{r_{\text{Residual}}} = \frac{\sigma_Y}{2}\left[\frac{a^2}{r^2} - 1\right] + \sigma_y \ell n \frac{r}{b} - \frac{\sigma_y a^2}{r^2} \ell n \frac{a}{b} \quad \text{for } a \le r \le b \tag{1a}$$

$$\sigma_{r_{\text{Residual}}} = -\frac{\sigma_y b^2}{2r^2} - \frac{\sigma_y a^2}{r^2} \ell n \frac{a}{b} + \frac{\sigma_y a^2}{2r^2} \quad \text{for } b \le r \tag{1b}$$

$$\sigma_{\theta_{\text{Residual}}} = \frac{\sigma_y}{2}\left[1 - \frac{a^2}{r^2}\right] + \sigma_y \ell n \frac{r}{b} + \frac{\sigma_y a^2}{r^2} \ell n \frac{a}{b} \quad \text{for } a \le r \le b \tag{2a}$$

$$\sigma_{\theta_{\text{Residual}}} = \frac{\sigma_y b^2}{2r^2} + \sigma_y \frac{a^2}{r^2} \ell n \frac{a}{b} - \frac{\sigma_y a^2}{2r^2} \quad \text{for } b \le r \tag{2b}$$

where σ_y is the yield stress, a is the radius of the hole, and b is the radius of the elastic-plastic interface. The radius b can be obtained from

$$u_{\text{final}} = u_{0e} + \frac{\sigma_y}{2E}\left[(3-\nu)\frac{a}{2}\left[\frac{b^2}{a^2} - 1\right] - 2(1-\nu)\, a \ell n \frac{b}{a}\right] \tag{3}$$

In this equation u_{final} is the largest radial displacement caused by the mandrel at $r=a$, E is the modulus of elasticity, ν is the Poisson's ratio, and u_{0e} is the radial displacement at $r=a$ when the incipient yielding takes place in the material.

$$u_{0e} = \sigma_y (1+\nu) a/2E \tag{4}$$

For the stress coined specimens discussed in this paper, $a=0.125$ in. $\sigma_y = 65{,}000$ psi, $E = 10.3 \times 10^6$ psi, and $\nu = 0.32$. Then

$$u_{0e} = 0.0005 \text{ in.} \tag{5}$$

From the mandrel geometry and the assumption of rigidity of the mandrel $u_{\text{final}} = 0.003$ in. Then, $b/a = 2.5$ from Eq. (3). The distribution of the residual stresses σ_r and σ_θ can be plotted as shown in Fig. 10. It can be seen that the maximum tensile stress (σ_θ) occurs at $r=b$ and is equal to 18,400 psi. This is larger than the threshold stress of 7000 psi necessary to cause stress corrosion cracking.

To investigate the validity of the theoretical developments, the portion of the stress coined and tested specimens where the hole spacing is 1¼ in. was selected. The chosen specimen had not shown any macrocracking on the surface. A large number of microcracks were observed at section $b/a = 2.5$ and 2.3 where the tensile stresses are above the threshold level according to the theoretical analysis.

Appendix

Investigations of the stress distribution resulting from the stress coining process is discussed in this Appendix. The Ap-

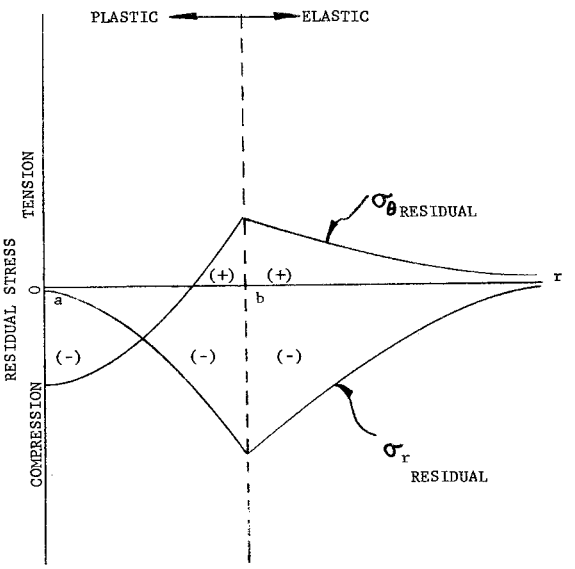

NOTE: a ~ EXPANDED HOLE RADIUS
b ~ ELASTIC-PLASTIC BOUNDARY
r ~ RADIAL DISTANCE

Fig. 10 Residual stress distribution.

pendix contains three sections. The first describes an elastic analysis to determine the minimum radial displacement caused by the mandrel (u_{0e}) necessary to cause the onset of yielding. The next section describes the elastic-plastic loading analysis to determine the stress produced when the mandrel has been fully inserted causing $u_f (u_f > u_{0e})$ at the hole. Finally, an elastic-unloading analysis is used to obtain the residual stresses remaining in the coined structure after the mandrel has been withdrawn completely from the hole. The authors are not aware of the solution to this problem reported elsewhere.

The analysis is done under the assumptions of Hooke's Law, small displacements, and plane stress conditions. Furthermore, cold worked material is assumed to be isotropic and ideally plastic. Tresca yield condition and the associated flow rules are assumed to be valid. The cold working mandrel is considered to be a rigid body and the fastener holes are assumed to be sufficiently spaced such that no interaction of the deformation occurs. The thickness variations in the plastic region are neglected.

Elastic Analysis

Figure 11 shows the schematic of stress-coined hole for elastic-plastic analysis. For elastic analysis, the radius $r=b$ coincides with $r=a$ and there is no plastic zone. The boundary conditions are as follows. At $r=a$ the radial displacement (u_0) is known since the cold working mandrel is assumed to be rigid. As the radial coordinate r tends to ∞, the radial normal stress $\sigma_r = 0$. Then, the well-known methods of elastic analysis[10] yield the following expressions for u, σ_r, and σ_θ (θ refers to the polar coordinate).

$$u = au_0/r \tag{A1}$$

$$\sigma_r = (E/1+\nu)\ (au_0/r^2) \tag{A2}$$

$$\sigma_\theta = (E/1+\nu)\ (au_0/r^2) \tag{A3}$$

By using the Tresca yield condition (i.e., $|\sigma_\theta - \sigma_r| = \sigma_y$) the limiting elastic displacement (u_{0e}) is given by the following expression

$$u_{0e} = \sigma_y (1+\nu) a/2E \tag{A4}$$

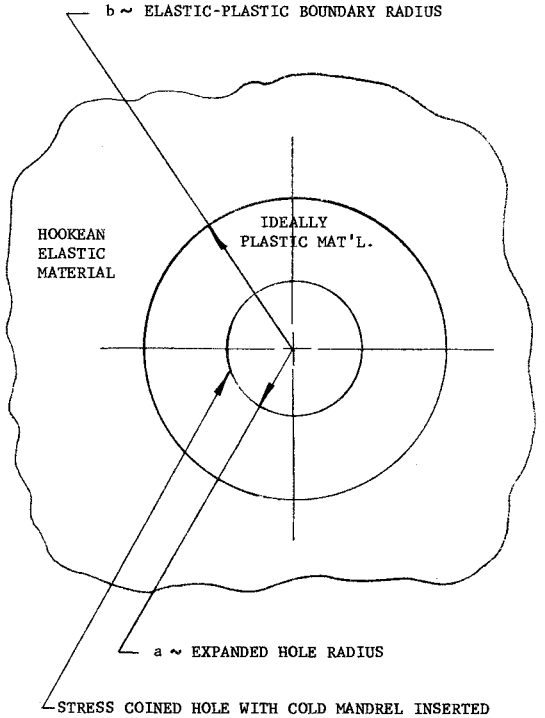

Fig. 11 Schematic of stress coined hole for elastic-plastic analysis.

Elastic-Plastic Loading Analysis

For $u_0 > u_{0e}$, the stress analysis should be based on the elastic-plastic behavior of the material. In Fig. 11, the radius $r=b$ denotes the elastic-plastic interface. The region $r \geq b$ is governed by elastic stress-strain relationship and the region $a \leq r \leq b$ needs the appropriate plasticity considerations. The stresses in the elastic zone must satisfy the following conditions

$$r \to \infty \qquad \sigma_{re} = 0 \tag{A5}$$

$$r = b \qquad \sigma_{\theta e} - \sigma_{re} = \sigma_y \tag{A6}$$

$$r = b \qquad \sigma_{re} = \sigma_{rp} \tag{A7}$$

In these equations, the subscript e refers to the stresses and displacements in the region $r \geq b$ and the subscript p denotes the quantity in the region $a \leq r \leq b$. The general expressions for $\sigma_{\theta p}$ and σ_{rp} that follow Tresca yield condition can be written[11] as

$$\sigma_{rp} = \sigma_y \ln r + c \tag{A8}$$

$$\sigma_{\theta p} = \sigma_y + \sigma_y \ln r + c \tag{A9}$$

where c is a constant. From Eqs. (A5-A9) and the well-known elastic solution, the expressions for stresses and displacements can be written in terms of the unknown interface radius $r=b$ as

$$\begin{aligned}
\sigma_{re} &= -\sigma_y b^2/2r^2 && r \geq b \\
\sigma_{\theta e} &= \sigma_y b^2/2r^2 && r \geq b \\
u_e &= [(1+\nu)/2E](\sigma_y b^2/r) && r \geq b \\
\sigma_{rp} &= \sigma_y \ln(r/b) - (\sigma_y/y) && a \leq r \leq b \\
\sigma_{\theta p} &= (\sigma_y/2) + \sigma_y \ln(r/b) && a \leq r \leq b
\end{aligned} \tag{A10}$$

In order to determine b in terms of the displacement u_0 at $r=a$, the general expression for displacement u_p should be noted. This needs the consideration of the appropriate flow rules associated with the Tresca yield condition.[12] These flow rules can be obtained by using Koiter's generalized plastic potential

$$d\epsilon_{\theta p} = \lambda db; \quad d\epsilon_{rp} = \lambda db; \quad d\epsilon_{zp} = 0 \tag{A11}$$

Where λ is the plastic flow function and db is the incremental elastic-plastic boundary displacement, the total strain increment $d\epsilon_{\delta e l}$ in the plastic region $a \leq r \leq b$ is

$$d\epsilon_{rtp} = d\epsilon_{rep} + d\epsilon_{rp} \tag{A12}$$

$d\epsilon_{rep}$ and $d\epsilon_{\theta ep}$ follow Hooke's law. Then

$$d\epsilon_{rtp} + d\epsilon_{\theta tp} = (1-\nu/E)\ (d\sigma_r + d\sigma_\theta) \tag{A13}$$

For a boundary displacement $u_0 = \eta$, let the elastic-plastic boundary $b = b(\eta)$. Then the corresponding stresses and displacements are

$$\sigma_{re} = \sigma'_{re}(r,\eta); \quad \sigma_{\theta e} = \sigma'_{\theta e}(r,\eta); \quad u_e = u'_e(r,\eta) \tag{A14}$$

$$\sigma_{\theta_p} = \sigma'_{\theta p}(r,\eta); \quad \sigma_{rp} = \sigma'_{rp}(r,\eta); \quad u_p = u'_p(r\eta)$$

If the boundary displacement u_0 is now increased by $d\eta$ to the new value $\eta + d\eta$, the quantities b', u'_p, u'_e, σ'_{rp}, $\sigma'_{\theta p}$, σ'_{re}, and $\sigma'_{\theta e}$ change by db', du'_p, du'_e, $d\sigma'_{rp}$, $d\sigma'_{\theta p}$, $d\sigma'_{re}$, and $d\sigma'_{\theta e}$. Equation (A-10) can be rewritten by using strain-

displacement relations and

$$\frac{d}{dr}(du'_p)+\{1-\frac{2(1-\nu)}{E}\sigma_y\}\frac{du'_p}{r}=\frac{2(1-\nu)}{E}\frac{\sigma_y}{b'}db' \quad (A15)$$

For the test specimens examined during this investigation, $2(1-\nu)\sigma_y/E$ is equal to 0.0095, and it can be neglected when compared to 1. Then

$$du'_p=\frac{df}{r}-\sigma_y\frac{(1-\nu)}{E}\frac{r}{b'}db' \quad (A16)$$

where df is a constant of integration that can be determined by the boundary condition $du'_p=d\eta$ at $r=a$. Then du'_p, as a function b and η, can be written as

$$du'_p=\frac{a}{r}d\eta+\frac{(1-\nu)}{E}\sigma_y\left[\frac{a^2}{r}-r\right]\frac{1}{b'}db' \quad (A17)$$

To determine b as a function of the displacement $u_0=\eta$ at $r=a$, the condition of continuity of displacements at $r=b$

$$u_e(b,\eta)=u_p(b,\eta) \quad (A18)$$

Because $b=b\ (\eta)$ only, Eq. (A18) can be written along $r=b\ (\eta)$ as

$$\frac{du'_e}{d\eta}d\eta=\frac{du'_p}{d\eta}d\eta;\quad r=b\ (\eta) \quad (A19)$$

By substituting for du'_e and du'_p from Eqs. (A10) and (A17), the equation becomes

$$(\sigma_y/2E)\{(3-\nu)b'/a+2(1-\nu)a/b'\}db'=d\eta \quad (A20)$$

By integrating Eq. (A20) between the limits $b'=a$ to $b'=b$ and $\eta=u_{0e}$ to u_{final}

$$u_{\text{final}}=u_{0e}+(\sigma_y/2E)\{(3-\nu)(a/2)(b^2/a^2-1)-2(1-\nu)a\ln(b/a)\} \quad (A21)$$

For specific u_{final} provided by the mandrel, b can be determined from Eq. (A21). Then, stresses can be determined from Eq. (A10).

Unloading

During elastic unloading, i.e., withdrawing the mandrel, the governing equations for the resulting displacements and stresses are

$$u(r)=u_p(r)+c_6r+(c_7/r)\ \text{for}\ s\le r\ll b \quad (A22a)$$

$$u(r)=u_e(r)+c_8r+(c_9/r)\ \text{for}\ b\le r \quad (A22b)$$

$$\sigma_r(r)=\sigma_{rp}(r)+\frac{E}{1-\nu^2}\{c_6(1+\nu)-\frac{c_7}{r^2}(1-\nu)\}$$

$$\text{for}\ a\le r\le b \quad (A23a)$$

$$\sigma_r(r)=\sigma_{re}(r)+\frac{E}{1-\nu^2}\{c_8(1+\nu)-\frac{c_9}{r^2}(1+\nu)\}$$

$$\text{for}\ b\le r \quad (A23b)$$

In these equations $u_p(r)$, $u_e(r)$, $\sigma_{rp}(r)$, $\sigma_{re}(r)$, and b refer to the values attained in the material just before withdrawing the mandrel. The constants c_6-c_9 are obtained from the appropriate boundary conditions. σ_r is equal to zero for $r=a$ and $r=\infty$. $\sigma_{re}=\sigma_{rp}$ and $u_e=u_p$ at $r=b$. Then, the expression for stresses σ_r and σ_θ can be written as

$$\sigma_r(r)_{\text{Residual}}=\frac{\sigma_y}{2}\left(\frac{a^2}{r^2}-1\right)+\sigma_y\ln\frac{r}{b}-\frac{\sigma_y a^2}{r^2}\ln\frac{a}{b}$$

$$\text{for}\ a\le r\le b$$

$$\sigma_r(r)_{\text{Residual}}=-\frac{\sigma_y}{2}\frac{b^2}{r^2}-\sigma_y\frac{a^2}{r^2}\ln\frac{a}{b}+\sigma_y\frac{a^2}{2r^2}$$

$$\text{for}\ b\le r \quad (A24)$$

$$\sigma_\theta(r)_{\text{Residual}}=\frac{\sigma_y}{2}\left(1-\frac{a^2}{r^2}\right)+\sigma_y\ln\frac{r}{b}+\sigma_y\frac{a^2}{r^2}\ln\frac{a}{b}$$

$$\text{for}\ a\le r\le b$$

$$\sigma_\theta(r)_{\text{Residual}}=-\frac{\sigma_y b^2}{2r^2}+\sigma_y\frac{a^2}{r^2}\ln\frac{a}{b}-\frac{\sigma_y a^2}{2r^2}$$

$$\text{for}\ b\le r \quad (A25)$$

References

[1] Smith, C.R., "Preventing Fatigue Failures," *Assembly Engineering*, Hitchcock Publishing Co., Illinois, March, 1968.

[2] Speakman, E.R., "Fatigue Life Improvement through Stress Coining Methods," *Proceedings of the Symposium on Achievement of High Fatigue Resistance in Aluminum Alloys*, ASTM STP 467, American Society for Testing Materials, 1970, pp. 209-226.

[3] Hills, J. F., "Advances of Some New Fastener Systems," *SAE Transactions*, 68-02-06, 1968

[4] Dieter, G. E., *Mechanical Metallurgy*, McGraw-Hill, New York, 1961.

[5] Smallman, R. E., *Modern Physical Metallurgy*, Butterworths, London, 1963.

[6] Sprowls, D.O. and Brown, R.H., "Stress Corrosion Mechanism in Aluminum Alloys," *Proceedings of the International Conference on Fundamental Aspects of Stress Corrosion Cracking*, National Association of Corrosion Engineers, 1969, pp. 446-505.

[7] "Laboratory Immersion Corrosion Testing," ASTM G31-72, American Society for Testing and Materials, Philadelphia, Pa.

[8] "Stress Corrosion Test for Aluminum Alloy Plate Extrusions and Forging by Alternate Immersion, in *Metal Test Standards*, Standard 1516, Method 825, General Services Administration Specification Activity, Materials and Supplies Division, Naval Weapons Plant, Washington D.C.

[9] Phillips, A., Kerlins, V., and Whiteson, B.V.," *Electron Fractography Handbook*, Technical Rept. M. L. TDR-64-416, Jan. 1965, Airforce Materials Lab., Wright-Patterson Air Force Base, Ohio.

[10] Hill, R., *The Mathematical Theory of Plasticity*, The Clarendon Press, Oxford, England, 1950.

[11] Prager, W., "On the Use of Singular Yield Conditions and Associated Flow Rules," *Journal of Applied Mechanics*, Sept. 1953, Vol. 23, pp. 317-320.

[12] Fung, W. C., *Foundations of Solid Mechanics*, Prentice-Hall, Englewood, Cliffs, N.J., 1965, p. 146.